Low-energy magnetic excitation spectrum of the unconventional ferromagnet $CeRh_3B_2$

S. Raymond,[1] J. Panarin,[1] F. Givord,[1] A. P. Murani,[2] J. X. Boucherle,[3] and P. Lejay[3]
[1]*SPSMS, UMR-E 9001, CEA-INAC/UJF-Grenoble 1, 38054 Grenoble, France*
[2]*Institut Laue Langevin, 38042 Grenoble Cedex, France*
[3]*Institut Néel, CNRS, 38042 Grenoble Cedex, France*
(Received 28 July 2010; published 10 September 2010)

The magnetic excitation spectrum of the unconventional ferromagnet $CeRh_3B_2$ was measured by inelastic neutron scattering on single-crystal sample in the magnetically ordered and paramagnetic phases. The spin-wave excitation spectrum evidences high exchange interaction along the c axis about two orders of magnitude higher than the ones in the basal plane of the hexagonal structure. Both strong out-of-plane and small in-plane anisotropies are found. This latter point confirms that considering the $J=5/2$ multiplet alone is not adequate for describing the ground state of $CeRh_3B_2$. Quasielastic scattering measured above T_{Curie} is also strongly anisotropic between the basal plane and the c axis and suggests localized magnetism.

DOI: 10.1103/PhysRevB.82.094416 PACS number(s): 75.50.Cc, 75.30.Ds, 29.30.Hs

I. INTRODUCTION

$CeRh_3B_2$ is a Ce-based intermetallic compound with quite unique properties. It is ferromagnetic while most of the other Ce-based compounds are antiferromagnetic. The easy axis is in the basal plane of the hexagonal structure and the saturation magnetization 0.4 μ_B is strongly reduced compared to free cerium ion value (2.14 μ_B). More striking is its huge Curie temperature, $T_{Curie}=115$ K, that is two orders of magnitude higher that what would be expected from applying the de Gennes scaling to $GdRh_3B_2$ ($T_{Curie}=90$ K).[1] Different theoretical models from itinerant to localized magnetism have been proposed to explain the peculiarities of this compound and they are reviewed in the recent calculations.[2,3] The key ingredient is certainly the very short Ce-Ce distance (3.08 Å) along the c axis that leads to the proposition of strong interatomic Ce-4f-Ce-5d hybridization or even direct Ce-4f-Ce-4f interaction.[4] While initially itinerant magnetism was favored, many experimental results point toward localized 4f electrons with strong hybridization as inferred from photoemission spectroscopy,[5] NMR,[6] de Haas–van Alphen measurements.[7] Polarized neutron-diffraction and crystal-field spectroscopies give an evidence of a mixing of $J=5/2$ and $J=7/2$ multiplets in the ground-state wave function.[8,9] Compton scattering experiments[10,11] show that the orbital-to-spin-moment ratio is less than the expected value for Ce^{3+} ion. Hence the spin magnetism is enhanced in $CeRh_3B_2$ with respect to the orbital part and this could explain partly the high Curie temperature since exchange interactions couple spins. These overall features together with the strong recent interest for other f electron ferromagnetic systems, namely, the new uranium-based ferromagnetic superconductors,[12] motivated us to investigate the spin dynamics of $CeRh_3B_2$. It is worthwhile to note that no trace of superconductivity was detected when ferromagnetism is suppressed at 7 GPa (Ref. 13) in $CeRh_3B_2$ while superconductivity is known to exist in $Ce(Rh_{1-x}Ru_x)_3B_2$ for $0.62<x<1$ and ferromagnetism disappears for $x>0.16$.[14]

II. EXPERIMENTAL DETAILS

Experiments were carried out on the three-axis spectrometers IN12, IN22, IN20, and IN8 at Institut Laue Langevin, Grenoble. The configuration of each spectrometer is given in Table I. For all configurations, a fixed final energy was used together with a focusing analyzer without collimation. Except for IN8 where measurements were performed around (0,0,2), most measurements were carried out around the very weak nuclear reflection (0,0,1) in order to limit the contamination by acoustic phonons. The single crystal was grown by the Czochralski method by using isotopically enriched ^{11}B (90%) in order to reduce neutron absorption. The sample for neutron scattering consists of two coaligned platelets with [0,0,1] normal. Their thickness is 2 mm in order to reduce the effect of Rh neutron absorption. They are of typical length 25 mm and width 5 mm.

III. SPIN WAVES

Figure 1 shows magnetic excitation spectrum measured on IN12 at $\mathbf{Q}=(1,0,0)$ for $T=5$ and 150 K. They were fit with inelastic Lorentzian below T_{Curie} and quasielastic Lorentzian above T_{Curie} (see Appendix). These spectra give evidence of a gap in the excitation spectrum of about 2 meV for $\mathbf{q}=0$ in the ferromagnetic phase. [In this paper, $\mathbf{Q}=\tau+\mathbf{q}$, where τ is a zone center and $\mathbf{Q}=(Q_H,Q_K,Q_L)$ and $\mathbf{q}=(h,k,l)$]. The dispersion along the [1,0,0] direction was investigated by performing several constant $\mathbf{Q}$ scans. Figure 2 shows a representative magnetic excitation spectrum measured on IN20 at $\mathbf{Q}=(0.1,0,1)$ for 5 and 150 K. In this work, the background is consistently taken for each configuration

TABLE I. Instrument configurations. The given collimation is the one after the monochromator. Fixed final wave vector was used with a filter on the scattered beam. PG is pyrolitic graphite.

	Monoch.	Collim.	Anal.	Wave vector	Filter
IN12	PG	60′	PG	1.5	Be
IN22	PG	60′	PG	1.97, 2.662	PG
IN20	Si		PG	2.662	
IN8	Si		PG	4.1	PG
IN8	Cu		PG	4.1	PG

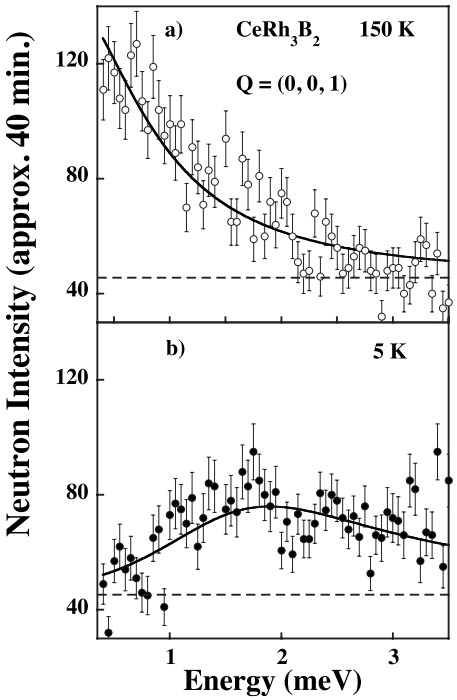

FIG. 1. Magnetic excitation spectrum of $CeRh_3B_2$ at $\mathbf{Q}=(0,0,1)$ for (a) $T=150$ K and (b) $T=5$ K. Solid lines are fit to the data with a quasielastic Lorentzian at 150 K and an inelastic Lorentzian at 5 K (see Appendix). The dashed line indicates the background.

as the flat part of the constant-energy and constant **Q** scans. The dispersion along the [0,0,1] direction was measured by performing constant-energy scans since the dispersion is much steeper in this direction than along [1,0,0]. Representative spectra are shown in Fig. 3. Figure 3(a) shows measurements performed on IN20 for an energy transfer of

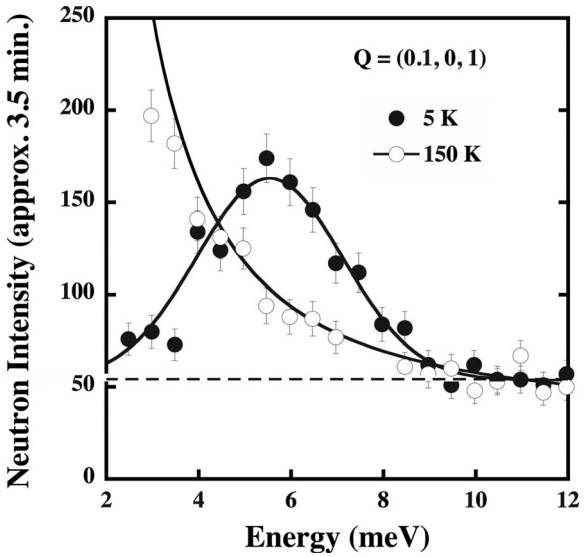

FIG. 2. Magnetic excitation spectrum of $CeRh_3B_2$ at $\mathbf{Q}=(0.1,0,1)$ for $T=5$ and 150 K. Solid lines are fit to the data with a quasielastic Lorentzian at 150 K and a Gaussian at 5 K (see Appendix). The dashed line indicates the background.

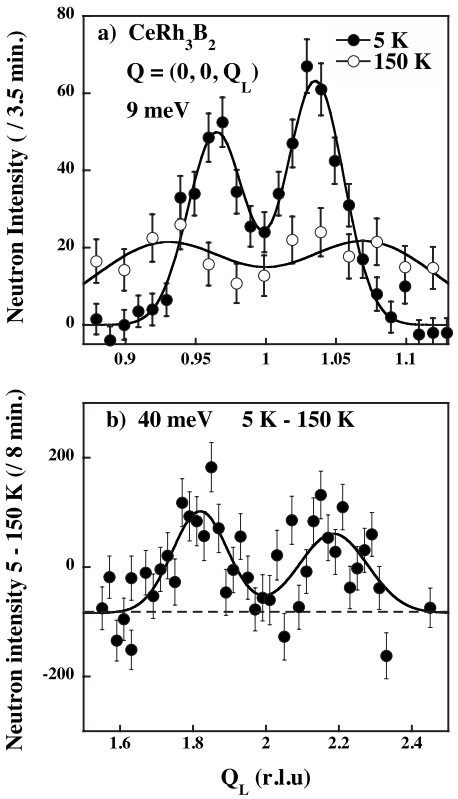

FIG. 3. (a) Constant-energy scans performed along [0,0,1] at 9 meV at 5 and 150 K with the background subtracted and corrected by the Bose factor. (b) Subtraction of the raw data measured at 5 and 150 K by constant-energy scan along [0,0,1] with energy transfer of 40 meV. Lines are fits with Gaussians (see Appendix).

9 meV subtracted from the background and corrected for the Bose factor. In the ferromagnetic phase, the asymmetry between the two peaks located on both sides of (0,0,1) corresponds to the defocusing and focusing conditions for the measurements. The data in the paramagnetic phase exhibit weak **Q** dependence due to magnetic correlations (see next part). Figure 3(b) shows a subtraction of the data measured at 5 and 150 K for an energy transfer of 40 meV on IN8. For this measurement the background is not well determined due to optic phonon and multiphonon contamination near (0,0,2) so that the same procedure as the one shown in Fig. 3(a) is not applied. However the peak position is still well defined. The resulting dispersion is shown in Fig. 4. There are three salient features: (i) the small gap at $\mathbf{q}=0$, (ii) the linear dispersion at small **q**, and (iii) the very high anisotropy of the spin-wave energy between the two directions. Without further analysis these facts already allow to draw some conclusions on the spin dynamics of $CeRh_3B_2$. Indeed for a ferromagnetic planar system, the spin-wave spectrum is linear and gapless. The observed gap is thus a signature of the in-plane anisotropy. Therefore, the spin wave is analyzed by using the following dispersion relation:[15]

$$\omega_q^2 = [\Delta_1 + 2SI(0) - 2SI(\mathbf{q})][\Delta_2 + 2SI(0) - 2SI(\mathbf{q})] \quad (1)$$

ω_q in the energy of the mode, Δ_1 is the axial anisotropy, and Δ_2 is the in-plane anisotropy. $I(\mathbf{q})$ is the Fourier transform of

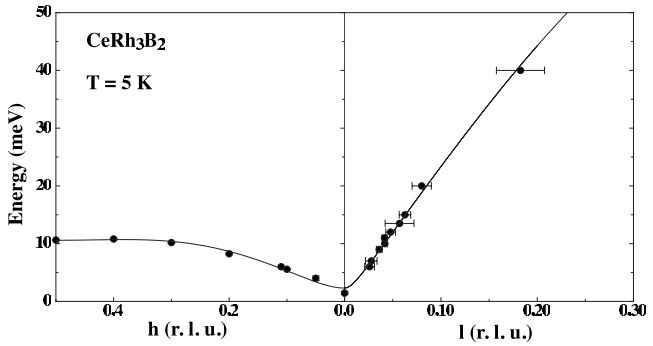

FIG. 4. Spin-wave dispersion in the [1,0,0] and [0,0,1] directions at 5 K. Lines are fit as explained in the text.

the exchange integral $I_{i,j}$ between the magnetic sites i and j with the Hamiltonian $\Sigma_{i,j}-I_{i,j}\mathbf{S}_i\mathbf{S}_j$. $\mathbf{S}_i$ is the spin operator at site i and S is the value of the spin. Table II shows the different exchange integrals and the corresponding distances between Ce atoms and the number of neighbors z. Given the shape of the dispersion, the relevant exchange parameters that we have deduced are: I_c the nearest-neighbor interaction along the c axis, I_1 the nearest-neighbor interaction in the basal plane and I_2, the next-nearest-neighbor interaction in the plane. Note that because measurement are performed only along [1,0,0] and [0,0,1], the exchange I_{diag} along [1,0,1] is included in I_c and I_1. If I_{diag} is strong (which is not really expected because the corresponding Ce-Ce distance is high), I_c and I_1 are effective parameters. We cannot also determine separately the exchange parameters and the energy gaps because they occur as products in Eq. (1). The obtained parameters from a fit of the dispersion shown in Fig. 4 are given in Table II. I_1 is not very well determined because part of I_2 intervenes in the same way as I_1 in the fit. The salient feature is the large difference between I_c and $I_1(I_2)$, the former being two orders of magnitude larger than the latter: $I_c/I_1 \approx 300$ and $I_c/I_2 \approx 100$. The dispersion along the [0,0,1] direction is characteristic of the regime $\Delta_1 > 2SI_c$ and good fits are indeed only obtained for $\Delta_1 > 100$ meV that leads also to the constraint $2SI_c < 20$ meV. We will tentatively give individual estimate for Δ_1 and I_c in the discussion part with extra hypotheses beyond the present fit. The gap at $\mathbf{q}=0$ is the geometric mean of the axial and in-plane anisotropies: $\omega_{q=0}=\sqrt{\Delta_1\Delta_2} \approx 2$ meV.

IV. PARAMAGNETIC SCATTERING

Preliminary data concerning paramagnetic scattering obtained on powder sample were shown in Ref. 9. A quasielastic signal was observed with a powdered average linewidth of 2 meV at 150 K and 5 meV at 300 K. Figure 5 shows representative spectra taken in the present single-crystal study at 120 K just above T_{Curie} for three wave vectors, which establishes the $\mathbf{Q}$ dependence of the signal. The data are analyzed with a quasielastic Lorentzian line shape convoluted with one-dimensional resolution in the ω direction. This analysis gives two parameters, the $\mathbf{q}$-dependent susceptibility χ_q and the relaxation rate Γ_q. In this work, the probed fluctuations are in-plane fluctuations since the wave vector has predominant component along the c axis [being $(h,0,1)$ or $(0,0,1+l)$] and neutron probes fluctuations perpendicular to $\mathbf{Q}$. The obtained relaxation rate is shown in Fig. 6 at 120 K and for [1,0,0] and [0,0,1] and for a few points at 150 K along [1,0,0]. The obtained values are qualitatively consistent with the powder averaged ones since the basal plane has more spectral weight than the c-axis direction. The extent in ω space of these excitations is smaller than that of the spin wave for the [0,0,1] direction and quite similar for the [1,0,0] direction. It seems that the relaxation rate extrapolates to zero for $\mathbf{q}=0$. However this is not expected since the in-plane magnetization is not a conserved quantity in a planar

TABLE II. Exchange integrals and anisotropies.

	Distance	Direction	z	Fit results	
I_1	5.48	[1,0,0]	6	$\Delta_1 2SI_1$	8(8) meV^2
I_2	9.49	[1,1,0]	6	$\Delta_1 2SI_2$	19(7) meV^2
I_c	3.04	[0,0,1]	2	$\Delta_1 2SI_c$	2520(40) meV^2
$I_{c'}$	6.08	[0,0,1]	2		
I_{diag}	6.26	[1,0,1]	6		
				$\Delta_1\Delta_2$	5(2) meV^2

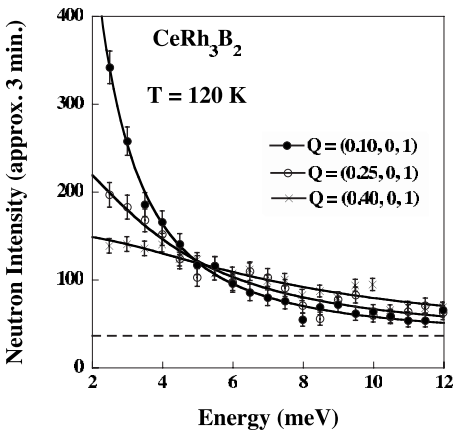

FIG. 5. Energy spectra measured at 120 K. Solid lines are fit to the data with a quasielastic Lorentzian (see Appendix). The dashed line indicates the background.

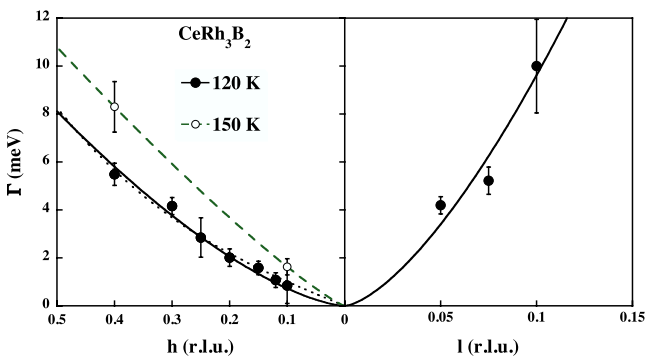

FIG. 6. (Color online) Relaxation rate in the [1,0,0] and [0,0,1] directions at 120 and 150 K. Lines are fit as explained in the text. The solid line corresponds to the local model and the dotted line corresponds to the itinerant model. The dashed line is a guide for the eyes.

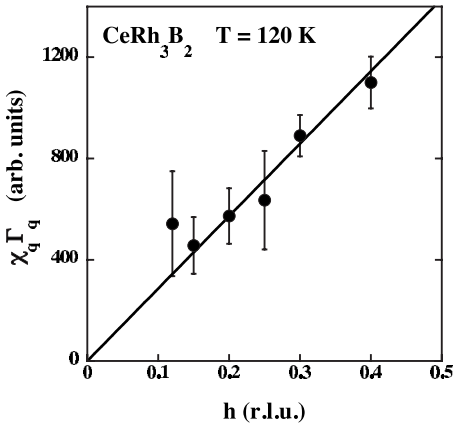

FIG. 7. The product $\chi_q\Gamma_q$ at 120 K for $\mathbf{q}$ along the [1,0,0] direction. The line is a linear fit going through the origin.

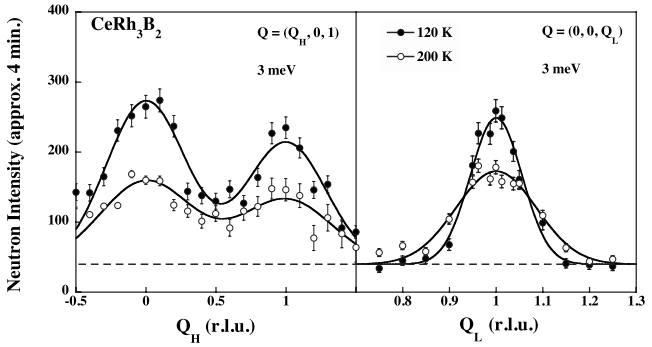

FIG. 8. Constant-energy scans performed for an energy transfer of 3 meV at 120 and 200 K along [1,0,0] and [0,0,1] directions. Solid lines are fit to the data with Gaussians as explained in the text. The dashed line indicates the background.

magnet.[16] Hence a small finite value $\Gamma_q(q=0)$ may exist but our data do not allow us to extract it. We fit the data obtained along the [1,0,0] direction at 120 K with either $\Gamma=Dh^z$ or $\Gamma=ah[1+(h/\kappa)^2]$ that corresponds, respectively, to localized or itinerant model of ferromagnetism. Along [1,0,0], we obtained $D=19(3)$ and $z=1.34(14)$ (solid line in Fig. 6) and, respectively, $a=9.9(9)$ meV(r.l.u.)$^{-1}$ and $\kappa=0.6(1)$ r.l.u. (dotted line in Fig. 6). It is worthwhile to note that z is close to 3/2, the dynamical exponent expected for an X-Y magnet.[16] The fit along the [0,0,1] direction is not exploited due to the limited number of data points. Usually the ratio D/T_{Curie} can give some information on the nature of the magnetism, i.e., localized versus itinerant. It is expected that $\langle\Gamma_q\rangle/T_{Curie}\gg 1$ for itinerant magnetism and that $\langle\Gamma_q\rangle/T_{Curie}\approx 1$ for localized magnetism.[17] This classification was applied for isotropic cubic magnets[18] or more recently in orthorhombic UGe_2.[19] It is highly questionable to apply it here since the value of D is quite different between the plane and the c axis (see Fig. 6). We could nevertheless notice that the powder-averaged value of the relaxation rate[9] leads to $\langle\Gamma_q\rangle/T_{Curie}<1$ that is in favor of localized magnetism. This conclusion is also sustained by the value of κ obtained by the itinerant model fit of Γ_q that is quite large for a temperature just above the Curie temperature and this analysis seems therefore unphysical. Hence our limited set of data obtained in the paramagnetic phase would suggest localized magnetism. Finally as compared to antiferromagnetic heavy-fermion systems where $\chi_q\Gamma_q$ is constant, it is worthwhile to point out that here $\chi_q\Gamma_q$ is almost linear in $\mathbf{q}$ for the [1,0,0] direction at 120 K for which data were extensively taken (see Fig. 7). This emphases the peculiarity of ferromagnetic fluctuations and the almost conserved magnetization. In the ferromagnetic compound UGe_2, it was found that $\chi_q\Gamma_q$ is linear with a large finite intercept at $q=0$.[20] Constant-energy scans performed for an energy transfer of 3 meV are shown in Fig. 8 for 120 and 200 K for [1,0,0] and [0,0,1] directions. The peak width is very anisotropic between the basal plane where peaks from adjacent Brillouin zones overlap and the c axis where peaks are narrow. The constant-energy scans can be fit by Lorentzian or Gaussian line shape and both fits provide almost the same width κ^*. This is not the true inverse correlation length κ since the measurement is performed for a finite energy of 3 meV while κ is obtained by energy-integrated imaginary part of the dynamical spin susceptibility. The Gaussian fit gives $\kappa^*_{[1,0,0]}=0.33(1)$ r.l.u., $\kappa^*_{[0,0,1]}=0.065(4)$ r.l.u. at 120 K and $\kappa^*_{[1,0,0]}=0.38(5)$ r.l.u., $\kappa^*_{[0,0,1]}=0.100(8)$ r.l.u. at 200 K. The temperature dependence of this characteristic length is more important along the c axis. This could explain the above-mentioned fact concerning the extent in $\mathbf{q}-\omega$ space of the fluctuations. The change in this extension along [0,0,1] between the paramagnetic and ordered phase could be due to a stronger temperature dependence of the different parameters in this direction. Exploiting further the paramagnetic scattering would need a detailed survey of the spin dynamics in the $(\mathbf{Q},\omega)$ space above T_{Curie}.

V. DISCUSSION

In this section, we give an estimate of I_c beyond the fit performed in Sec. III that only gave the constraint $2SI_c<20$ meV and $2S\Delta_1 I_c\approx 2500$. Knowing that $I_c\gg I_1, I_2$, it is tempting to describe the system as a set of weakly coupled ferromagnetic chains.[21] In such a model $I_c\gg T_{Curie}$ and three-dimensional order occurs for $T_{Curie}\approx 2S(S+1)\sqrt{I_cI_1}$ for six neighboring chains.[22] However here our spin-wave data show that $2SI_c<20$ meV. Knowing that $2S\sim 1$ from Compton scattering, we deduce that I_c is not much stronger than T_{Curie} and the weakly coupled ferromagnetic chains model is therefore not valid here. For the purpose of an estimate, we therefore use the usual mean-field approximation in its crude formulation, $T_{Curie}\approx I_c$, since I_c is the dominant coupling. [In such a case, the exact formula is $T_{Curie}=\frac{2z}{3}S(S+1)I_c$.] This leads to the following order of magnitudes: $I_c\approx 10$ meV, $\Delta_1\approx 250$ meV, and $\Delta_2\approx 0.02$ meV. This is to be compared to the value of the out-of-plane anisotropy inferred from the latest x-ray absorption spectroscopy results, $\Delta_1\approx 50$ meV.[23] The origin of the X-Y nature of the system is the strong crystal-field anisotropy. The dispersion relation given in formula (1) was used for exchange-dominated planar ferromagnets such as Tb (Ref. 24) with in this case the use of total angular momentum J instead of S. In such a case, the anisotropy gaps are expressed as $\Delta_1=6JB_2^0$ and $\Delta_2=36J_5B_6^6$ with

$J_n=J(J-1)\ldots(J-n/2)$ and B_b^a are the canonical coefficients of the crystal-field Hamiltonian when expressed with the Stevens formalism.[25] We cannot use this formulation for $CeRh_3B_2$ since for Ce^{3+} with a total momentum $J=5/2$ ground state, the coefficient B_6^6 is zero. As stated above, the gap at $q=0$ is a strong indication that in-plane anisotropy exists. For Ce^{3+} this is impossible with $J=5/2$. Hence the multiplet $J=7/2$ has to be taken into account in the ground-state wave function. This mixing between $J=5/2$ and $J=5/2$ in the ground state was first pointed out by the form-factor measurements.[8] Concerning the anisotropy in the plane, one of the reported magnetization measurements at 2 K found a difference of 0.004 μ_B for the saturated magnetization between a and a^* axes.[26] However this result was not reproduced by another group that also reports possible sample disorientation issue in the aforementioned work.[27] The small value of Δ_2 that we proposed here implies that its signature will only occur at very low temperature probably much below 2 K.

VI. CONCLUSION

In the present paper, we have focused on the magnetic interactions in $CeRh_3B_2$ while previous neutron-scattering studies focused on single-site crystal-field contributions. Usually rare-earth compounds are classified into exchange dominated or crystal-field-dominated systems.[24] This classification is clearly not valid for $CeRh_3B_2$ where all energy scales must be taken into account in the ground state and low-lying excitations: spin-orbit, crystal field, and exchange. While our study does not answer the question of the microscopic origin of the strong Curie temperature, we clearly establish the huge anisotropy between the exchange along the c axis and in the plane as well as the anisotropy within the plane that precludes a description of the magnetism in term of $J=5/2$ only. The spin-wave spectra extending presumably up to 80 meV at the c-axis zone boundary has the highest energy for any known cerium compound. This huge value is clearly a combination of crystal-field anisotropy (Δ_1) and exchange (I_c). The present work is aiming to stimulate further theoretical studies that would be able to treat on the same footing all the aspects (spin-orbit, crystal field, and exchange) of the intriguing magnetism of $CeRh_3B_2$.

APPENDIX

In a neutron-scattering experiment, the measured intensity is the convolution of the resolution function and the scattering function $S(\mathbf{Q},\omega)$. This latter function is related to the imaginary part of the dynamical spin susceptibility $\chi''(\mathbf{Q},\omega)$ via the fluctuation-dissipation theorem $S(\mathbf{Q},\omega)=[1-\exp(-\omega/T)]^{-1}\chi''(\mathbf{Q},\omega)$. In this paper, we use for the paramagnetic scattering [Figs. 1(a), 2, and 5], a "quasielastic Lorentzian:"

$$\chi''(\mathbf{q},\omega)=\frac{\chi_q\Gamma_q\omega}{\omega^2+\Gamma_q^2} \tag{2}$$

For the spectra measured at $\mathbf{Q}=(0,0,1)$ [Fig. 1(b)], we use the following form, that was named "inelastic Lorentzian" in the paper:

$$\chi''(\mathbf{q},\omega)=\frac{1}{2}\left[\frac{\chi_q\Gamma_q\omega}{(\omega-\omega_0)^2+\Gamma_q^2}+\frac{\chi_q\Gamma_q\omega}{(\omega+\omega_0)^2+\Gamma_q^2}\right] \tag{3}$$

This form is phenomenologically used to reproduce the broadening of the peak. The origin of this anomalous shape is presumably the steep dispersion along the c axis that is picked up by the finite-resolution function. This effect is strongest at the minimum of the dispersion. For the spin-wave spectra at finite $\mathbf{q}$, we use a Gaussian for $S(\mathbf{Q},\omega)$ both for the constant $\mathbf{Q}$ (Fig. 2) and constant ω (Fig. 3) scans, i.e., for $x=h$, l, or ω.

$$S(\mathbf{q},\omega)=S(x)=I\exp\{-\ln 2[(x-C)/W/2]^2\} \tag{4}$$

with I the peak intensity, C the position of the peak and W its full width at half maximum (in $\mathbf{Q}$ or ω space).

[1] S. K. Dhar, S. K. Malik, and R. Vijayaraghavan, J. Phys. C **14**, L321 (1981).

[2] K. Yamauchi, A. Yanase, and H. Harima, J. Phys. Soc. Jpn. **79**, 044717 (2010).

[3] H. N. Kono and Y. Kuramoto, J. Phys. Soc. Jpn. **75**, 084706 (2006).

[4] See, e.g., K. Takegahara, H. Harima, and T. Kasuya, J. Phys. Soc. Jpn. **54**, 4743 (1985).

[5] A. Fujimori, T. Takahashi, A. Okabe, M. Kasaya, and T. Kasuya, Phys. Rev. B **41**, 6783 (1990).

[6] Y. Kishimoto, Y. Kawasaki, and T. Ohno, J. Phys. Soc. Jpn. **73**, 1970 (2004).

[7] T. Okubo, M. Yamada, A. Thamizhavel, S. Kirita, Y. Inada, R. Settai, H. Harima, K. Takegahara, A. Galatanu, E. Yamamoto, and Y. Ōnuki, J. Phys.: Condens. Matter **15**, L721 (2003).

[8] F. Givord, J.-X. Boucherle, E. Lelièvre-Berna, and P. Lejay, J. Phys.: Condens. Matter **16**, 1211 (2004).

[9] F. Givord, J.-X. Boucherle, A. P. Murani, R. Bewley, R.-M. Galéra, and P. Lejay, J. Phys.: Condens. Matter **19**, 506210 (2007).

[10] A. Yaouanc, P. Dalmas de Réotier, J.-P. Sanchez, Th. Tschentscher, and P. Lejay, Phys. Rev. B **57**, R681 (1998).

[11] Y. Sakurai, M. Itou, J. Tamura, B. Nanao, A. Thamizhavel, Y. Inada, A. Galatanu, E. Yamamoto, and Y. Ōnuki, J. Phys. Condens. Matter **15**, S2183 (2003).

[12] See, e.g., D. Aoki, T. D. Matsuda, V. Taufour, E. Hassinger, G. Knebel, and J. Flouquet, J. Phys. Soc. Jpn. **78**, 113709 (2009) and references therein.

[13] A. L. Cornelius and J. S. Schilling, Phys. Rev. B **49**, 3955 (1994).

[14] J. W. Allen, M. B. Maple, J.-S. Kang, K. N. Yang, M. S. Torikachvili, Y. Lassailly, W. P. Ellis, B. B. Pate, and I. Lindau, Phys. Rev. B **41**, 9013 (1990).

[15] K. Niira, Phys. Rev. **117**, 129 (1960).

[16] S. Thoma, E. Frey, and F. Schwabl, Phys. Rev. B **43**, 5831 (1991), and references therein.
[17] T. Moriya, *Spin Fluctuations in Itinerant Electron Magnetism* (Springer-Verlag, Berlin, 1985).
[18] For a review, see Y. Endoh and P. Böni, J. Phys. Soc. Jpn. **75**, 111002 (2006).
[19] S. Raymond and A. Huxley, Physica B **350**, 33 (2004).
[20] A. D. Huxley, S. Raymond, and E. Ressouche, Phys. Rev. Lett. **91**, 207201 (2003).
[21] M. Steiner, J. Villain, and C. G. Windsor, Adv. Phys. **25**, 87 (1976).
[22] D. J. Scalapino, Y. Imry, and P. Pincus, Phys. Rev. B **11**, 2042 (1975).
[23] K. Yamaguchi, H. Namatame, A. Fujimori, T. Koide, T. Shidara, M. Nakamura, A. Misu, H. Fukutani, M. Yuri, M. Kasaya, H. Suzuki, and T. Kasuya, Phys. Rev. B **51**, 13952 (1995).
[24] A. R. Mackintosh, J. Magn. Magn. Mater. **15-18**, 236 (1980).
[25] K. W. H. Stevens, Proc. R. Soc. London, Ser. A **65**, 209 (1952).
[26] A. Galatanu, E. Yamamoto, T. Okubo, M. Yamada, A. Thamizhavel, T. Takeuchi, K. Sugiyama, Y. Inada, and Y. Ōnuki, J. Phys.: Condens. Matter **15**, S2187 (2003).
[27] F. Givord, J.-X. Boucherle, R.-M. Galéra, G. Fillion, and P. Lejay, J. Phys.: Condens. Matter **19**, 356208 (2007).